High-energy forward elastic scattering of electrons: Partial-wave approximations

R. K. Nesbet
IBM Research Laboratory, San Jose, California 95193

S. Geltman
Joint Institute for Laboratory Astrophysics, National Bureau of Standards and University of Colorado, Boulder, Colorado 80309

(Received 22 May 1984; revised manuscript received 3 March 1986)

Partial-wave analysis is applied to a parametrized pseudostate excitation model of high-energy electron-atom scattering. Consistency checks are carried out between asymptotic distorted-wave calculations (for coupled differential equations), second-Born-approximation scattering amplitude calculations, and partial-wave second-Born-approximation calculations. Closure formulas for partial-wave amplitude sums are derived for a static model potential and for the second-Born-approximation amplitude due to the asymptotic dipole excitation potential. Calculations using these closure formulas in e^- + H and e^- + Ar models at 15 keV show cusplike forward elastic scattering peaks, confirming recent exact second-Born-approximation results for an e^- + H pseudostate model. Using parameters appropriate to ground-state rare-gas atoms, the computed forward peaks are much too small to account for recent experimental observations. The theory indicates that these structures increase in magnitude rapidly with atomic radius, suggesting that the observed strong forward peaks may arise from excited atoms or ions in the electron beam path.

I. INTRODUCTION

Geiger and Morón-León[1] have reported experimental observations of strong forward peaks, with structure similar to a Fraunhofer diffraction pattern, in the cross section for elastic scattering of 15—25-keV electrons by rare-gas atoms. A strong forward peak, whose magnitude increases with impact energy, is reported for elastic scattering by He of 10—25-keV electrons.[2]

In order to see if such diffraction peaks might follow from a realistic theory, exact second-Born-approximation calculations[3,4] and partial-wave calculations were carried out for a polarization pseudostate model of atomic hydrogen. Although a forward elastic scattering peak is obtained in these calculations, its magnitude agrees with that expected from prior second-Born-approximation calculations,[5–8] much too small to agree with the experimental data. These theoretical results differ by several orders of magnitude from earlier partial-wave calculations by Mohr.[9] In the present paper, the pseudostate model is used to examine the relationship between the partial-wave expansion and second-Born-approximation theory.

Because the experimental data[1] appear to disagree with Born-approximation theory, it is important to make sure that there is no fundamental error made in truncating the Born-approximation expansion at low order. The present partial-wave calculations agree with the second Born approximation for extreme forward elastic scattering in the high-energy limit, confirming analysis of the Born-approximation expansion.[7] In the present work, the methodology ensures that residual sums of partial-wave series are not neglected. Such neglect might be a serious source of error, since the relevant series are very slowly convergent. The present systematic treatment of high-order partial waves may account for the large difference between present results and those of Mohr.[9] Although the present results exclude interpretation of the observed forward scattering peaks[1,2] as elastic scattering from ground-state atoms, they also indicate that very much larger effects would be obtained if excited atoms were present in the path of the electron beam.

The detailed analysis given here of relations between partial-wave calculations and second-Born-approximation or optical potential theory is itself of interest, since it can be used at much lower scattering energies to provide closure formulas for partial-wave sums.

The theoretical model is described in Sec. II. Partial-wave analysis and approximations used here are discussed in Sec. III. Asymptotic distorted-wave calculations[10] are described in Sec. IV. Results of partial-wave calculations are presented in Sec. V and discussed in Sec. VI.

II. DESCRIPTION OF MODEL

Electron-impact excitation from an atomic orbital s state to a p state (dipole excitation pseudostate) is modeled. The target radial wave functions, $u_0(r)$ and $u_p(r)$, respectively, define a reduced transition moment

$$\mu = -(u_p \mid r \mid u_0) , \tag{1}$$

in atomic units, and correspond to an excitation energy

$$\Delta E_p = E_p - E_0 . \tag{2}$$

The momentum or wave number of the scattered electron in the ground state and pseudostate channel, respectively, is determined by

$$k^2=2(E-E_0)=2E_i\ , \tag{3}$$

$$k_p^2=2(E-E_p)=2(E_i-\Delta E_p)\ . \tag{4}$$

Here E_i is the incident energy in the ground-state channel, and E is the total energy.

The excitation process is described in first order by differential equations that couple the channel orbital function $f_l(r)$ of the ground state, for partial-wave angular momentum, l, to pseudostate channel orbital functions $g_{l'}(r)$, where $l'=l\pm1$. Following Burke *et al.*,[11] the close-coupling equations (without exchange) can be derived for coupled magnetic substates $(lm),(l'm')$. With the assumption that f_l and $g_{l'}$ are independent of m or m', these equations can be combined with vector coupling coefficients to give reduced differential equations for the channel orbital functions. In the asymptotic region, where r is large enough to justify neglect of exponentially decreasing potential functions, the reduced equations are

$$\left[\frac{d^2}{dr^2}-\frac{l(l+1)}{r^2}+k^2\right]f_l(r) =\frac{2}{\sqrt{3}}\frac{\mu}{r^2}[\gamma_{l-1}g_{l-1}(r)+\gamma_{l+1}g_{l+1}(r)]\ , \tag{5a}$$

$$\left[\frac{d^2}{dr^2}-\frac{l'(l'+1)}{r^2}+k_p^2\right]g_{l'}(r) =\frac{2}{\sqrt{3}}\frac{\mu}{r^2}\gamma_{l'}f_l(r),\quad l'=l\pm1\ , \tag{5b}$$

where

$$\gamma_{l-1}=[l/(2l+1)]^{1/2}\ ,\qquad \gamma_{l+1}=[(l+1)/(2l+1)]^{1/2}\ . \tag{6}$$

Note that g_{l-1} does not appear if $l=0$.

For agreement with the analytic pseudostate model of atomic hydrogen, Eqs. (5) must be modified at small r. The right-hand member of Eq. (5a) for the ground-state channel is augmented by two terms,[4]

$$2v_{00}(r)f_l(r)+\frac{2}{\sqrt{3}}\mu\Delta v_{p0}(r)\sum_{l'}\gamma_{l'}g_{l'}(r)\ , \tag{7}$$

where

$$v_{00}(r)=-e^{-2r}\left[1+\frac{1}{r}\right]\ , \tag{8}$$

and

$$\Delta v_{p0}(r)=-e^{-2r}\left[\frac{2}{9}r^2+\frac{10}{9}r+2+\frac{2}{r}+\frac{1}{r^2}\right]\ . \tag{9}$$

Equation (9), an exact result for the pseudostate model,[4] provides a smooth cutoff for $1/r^2$ at small r in the dipole transition potential. Similarly, in Eq. (5b), $1/r^2$ should be replaced by $1/r^2+\Delta v_{p0}(r)$ at small r.

In the present work, concerned with elastic scattering in the ground-state channel, the short-range potential $v_{pp}(r)$ in the pseudostate channels is neglected. In contrast, $v_{00}(r)$, acting in the ground-state channel, is taken into account explicitly. The off-diagonal dipole screening potential $\Delta v_{p0}(r)$ is important only for partial waves of low order, $l<kr_0$, where r_0 is an effective ground-state atomic radius. To simplify the calculations, this short-range cutoff is simulated by computing matrix elements of the unscreened potential μ/r^2 when $l\geq kr_0$, using a scaling approximation to estimate the screened matrix elements for smaller l.

III. PARTIAL-WAVE APPROXIMATIONS

At low impact energies it is feasible to integrate Eqs. (5) numerically, including short-range potentials for low l values. At high energies, the number of partial waves that must be considered becomes large, and numerical integration of rapidly oscillatory functions becomes increasingly difficult. The practical approach is to integrate the differential equations only for small l, making use of the partial-wave Born approximation for larger l. At any given impact energy, the partial-wave Born approximation is accurate for sufficiently large l.

The elastic scattering amplitude $f(\theta)$ is expressed in terms of partial-wave transition matrix elements T_{ll} by the sum

$$f(\theta)=\sum_{l=0}^{\infty}\frac{2l+1}{k}T_{ll}P_l(\cos\theta)\ . \tag{10}$$

Closure formulas for this sum can be derived when both $f(\theta)$ and T_{ll} can be evaluated up to some order of Born approximation, with values given by $f^{(B)}(\theta)$ and $T_{ll}^{(B)}$, respectively. If $T_{ll}^{(B)}$ is an accurate approximation to the true T_{ll} for l greater than some value l_B, then Eq. (10) can be replaced by

$$f(\theta)=f^{(B)}(\theta)+\sum_{l=0}^{l_B}\frac{2l+1}{k}(T_{ll}-T_{ll}^{(B)})P_l(\cos\theta)\ , \tag{11}$$

which truncates the partial-wave sum. This can be expressed as a closure correction

$$\Delta f(\theta)=f^{(B)}(\theta)-\sum_{l=0}^{l_B}\frac{2l+1}{k}T_{ll}^{(B)}P_l(\cos\theta) \tag{12}$$

to the truncated sum computed with T_{ll} elements.

Equation (12) was used by Thompson[12] to sum partial-wave amplitudes for the static polarization potential of rare-gas atoms. If the static electric dipole polarizability is α, $f^{(B1)}(\theta)$ and $T_{ll}^{(B1)}$ for the static polarization potential give

$$\Delta f(\theta)=\pi\alpha k\left[\frac{1}{3}-\frac{1}{2}\sin\frac{\theta}{2} -\sum_{l=1}^{l_B}\frac{1}{(2l+3)(2l-1)}P_l(\cos\theta)\right]\ , \tag{13}$$

making use of the formulas

$$T_{ll}^{(B1)}=K_{ll}^{(B1)}(\text{pol})=\frac{\pi\alpha k^2}{(2l+3)(2l+1)(2l-1)}\ , \qquad l>0 \tag{14}$$

and

$$\tfrac{1}{2}\sin(\theta/2)=-\sum_{l=0}^{\infty}\frac{1}{(2l+3)(2l-1)}P_l(\cos\theta)\ . \tag{15}$$

Singularities due to the r^{-4} potential cancel here between the two terms of $f^{(B1)}(\theta)-(1/k)T_{00}^{(B1)}$.

At impact energies of interest here (15—35 keV), Eq. (14) becomes a good approximation only for very large values of l. An estimate of l_B can be obtained by considering the optical potential valid in the elastic scattering channel for solutions of Eqs. (5). When asymptotic solutions are generated, using the method of Burke and Schey[13] or of Gailitis,[14] the right-hand side of Eq. (5a) can be converted directly into an asymptotic expansion of the elastic optical potential.[15] For energies above the excitation threshold E_p, the leading terms at large r are[3]

$$V^{\rm opt}(r)=\tfrac{1}{2}\alpha\left[-r^{-4}+\frac{2ik}{\Delta E_p}r^{-5}+O(r^{-6})\right], \tag{16}$$

in terms of the static dipole polarizability

$$\alpha=\tfrac{2}{3}\mu^2/\Delta E_p\ . \tag{17}$$

Equation (14) is a valid estimate of T_{ll} only for l values greater than $l_B=kr_B$, where r_B is the impact parameter beyond which the r^{-4} term in $V^{\rm opt}$ is dominant, and can be estimated as the value for which the r^{-4} and r^{-5} terms have equal magnitude. This implies

$$l_B=kr_B\cong 2k^2/\Delta E_p\ . \tag{18}$$

For sufficiently small impact energy, both l_B and r_B are small. In this limit the screened polarization potential

$$V^{\rm opt}(r)\cong-\tfrac{1}{2}\alpha[r^{-2}+\Delta v_{p0}(r)]^2\ , \tag{19}$$

a bounded function with correct asymptotic behavior, provides an effective potential with no free parameters. This is not a useful approximation at the energies considered here, for which l_B is very large. In Hartree atomic units the excitation energy of the hydrogen pseudostate is

$$\Delta E_p=\tfrac{18}{43}\ . \tag{20}$$

At 15 keV, the value of l_B, from Eq. (18), is 5270 and the impact parameter r_B is $159a_0$.

Since the imaginary part of the optical potential represents flux loss to inelastic scattering, the expected effect on the elastic scattering amplitude is to reduce its magnitude, in analogy to scattering by a black disk of radius r_B. In the partial-wave sum, the magnitude of T_{ll} should be reduced for $l<l_B$. If this cutoff were sharp, the real part of the elastic scattering amplitude would contain the truncated sum over partial-wave amplitudes given by Eq. (13). This functional form describes a forward peak, decreasing as a linear function of momentum transfer at $\theta=0$, with diffraction structure concentrated within an angle $2\pi/l_B$ determined by the residual term in a truncated expansion of Eq. (15). Since l_B increases with k, the magnitude of this forward peak necessarily decreases with increasing impact energy.

As an alternative to evaluating explicit partial-wave sums for large l_B, it is possible to use Eq. (11) for the second-Born-approximation scattering amplitude. The indirect amplitude $f_p^{(B2)}(\theta)$, appropriate to the asymptotic dipole excitation potentials of Eqs. (5), can be evaluated in closed form. Details are given in Appendix A. Partial-wave analysis of $f_p^{(B2)}(\theta)$ leads to formulas for T-matrix elements,

$$\mathrm{Re}\,T_{ll}^{(B2)}=\frac{1}{\pi}\mathrm{P}\int_0^{\infty}\frac{d\epsilon'}{\epsilon'-\epsilon_p}\sum_{l'}|\,T_{l'l}^{(B1)}(k',k)\,|^2\ , \tag{21}$$

where P denotes a principal value integral, and

$$\mathrm{Im}\,T_{ll}^{(B2)}=\sum_{l'}|\,T_{l'l}^{(B1)}(k_p,k)\,|^2\ . \tag{22}$$

From Eqs. (5) the required first-Born-approximation transition matrix element is

$$T_{l'l}^{(B1)}(k_p,k)=-\frac{2\mu}{\sqrt{3}}\gamma_{l'}\left\langle F_{l'}\left|\frac{1}{r^2}\right|F_l\right\rangle\ ,\quad l'=l\pm1\ , \tag{23}$$

where F_l is a regular solution of the radial free-particle equation, such that

$$F_l(k,r)=k^{1/2}rj_l(kr)\ . \tag{24}$$

In order to ensure unitarity (flux conservation), partial-wave calculations should be carried out in terms of the reactance matrix $K_{l'l}$ rather than the transition matrix $T_{l'l}$. Unitarity of the scattering matrix is assured if the K matrix is real and symmetric. Analysis of the scattering equations gives exact formulas, derived from matrix Lippmann-Schwinger equations,[16] for elements of the 3×3 K matrix,

$$K_{ll}=-\frac{2\mu}{\sqrt{3}}\left\langle F_l\left|\frac{1}{r^2}\right|\sum_{l'}\gamma_{l'}g_{l'}\right\rangle\ , \tag{25}$$

$$K_{l'l}=-\frac{2\mu}{\sqrt{3}}\left\langle F_{l'}\left|\frac{1}{r^2}\right|\gamma_{l'}f_l\right\rangle\ . \tag{26}$$

Elements $K_{l'l'}$ are not used here ($l'=l\pm1$). When elastic scattering is weak, $f_l(r)$ can be approximated by $F_l(k,r)$, and Eq. (26) reduces to

$$K_{l'l}^{(B1)}=T_{l'l}^{(B1)}\ , \tag{27}$$

given by Eq. (23). Similarly, when the solution of Eqs. (5) is expressed in terms of a principal-value Green's function, Eq. (25) reduces to

$$K_{ll}^{(B2)}=\mathrm{Re}\,T_{ll}^{(B2)}\ , \tag{28}$$

given by Eq. (21).

The integral for $T_{l'l}^{(B1)}$, Eq. (23), can be evaluated in closed form, as shown in Appendix B. If r_0 is an effective atomic radius, $T_{l'l}^{(B1)}$ must be modified for $l<kr_0$ to take into account the screening of $1/r^2$ by $\Delta v_{p0}(r)$. This behavior is simulated by use of a scaling formula, discussed in Appendix B. Evaluation of $\mathrm{Re}\,T_{ll}^{(B2)}$ or $K_{ll}^{(B2)}$ is also discussed in Appendix B. Because an explicit formula is known for $f_p^{(B2)}(\theta)$, alternative values of $\mathrm{Re}\,T_{ll}$ and $\mathrm{Im}\,T_{ll}$ can be obtained by inverting the partial-wave expansion, to give

$$T_{ll}^{(B2)}=\frac{k}{2}\int_{-1}^{+1}f_p^{(B2)}(\cos^{-1}x)P_l(x)dx\ , \tag{29}$$

also discussed in Appendix B.

The present analysis indicates that for given k three ranges of l must be considered. For $l < kr_0$, short-range potentials cannot be neglected. In this range $T_{ll}^{(B1)}$ is computed for the static potential $v_{00}(r)$, Eq. (8). Evaluation of the required integrals is discussed in Appendix C. Since both $f^{(B1)}(\theta)$ and $T_{ll}^{(B1)}$ can be evaluated for $v_{00}(r)$, Eq. (11) is used to complete the sum of partial waves $l \geq kr_0$. The screening of the dipole transition potential due to $\Delta v_{p0}(r)$, Eq. (9), is taken into account for $l < kr_0$ by scaling the matrix elements $T_{l'l}^{(B1)}$, as described in Appendix B.

Consistent with identifying Eqs. (C1) and (21) as estimates of K-matrix elements, which can be denoted by $K_{ll}(0)$ and $K_{ll}(p)$, respectively, these elements are combined for $l < kr_0$ by adding effective phase shifts. The implied formula is

$$K_{ll} = \frac{K_{ll}(0) + K_{ll}(p)}{1 - K_{ll}(0)K_{ll}(p)} . \tag{30}$$

In preliminary calculations, used to verify the formulas given here over a large range of l values, the residual sum over partial-wave amplitudes for $l \geq l_B$ with l_B estimated by Eq. (18) was replaced by (13). Equations (31) and (23) were evaluated in the intermediate range $kr_0 \leq l < l_B$. This provided a check on the final calculations reported here, in which $f_p^{(B2)}$ was used for closure in Eq. (11), and convergence of the partial-wave sum was found with much smaller $l_B \gtrsim kr_0$.

IV. ASYMPTOTIC DISTORTED-WAVE CALCULATIONS

At very small scattering angles, short-range potentials do not produce angular structure in the differential cross section. Hence, in seeking an explanation of an observed forward scattering peak apparently much greater in magnitude than that found in second-Born-approximation amplitude calculations, exact treatment of short-range potentials is not required. To examine the validity of Born approximations for $K_{ll}^{(B2)}$ and for transition elements $K_{l'l}^{(B1)}$, calculations were carried out using an asymptotic distorted-wave model (ADW), to be described here.

The coupled differential equations, Eqs. (5) can be solved accurately for $r > r_0$ using a combination of methods. For sufficiently large r, the Gailitis expansion[14] is used, with convergence accelerated by converting the resulting series in powers of r^{-1} into continued fractions.[17] Solutions are carried out from r_0 out to the Gailitis boundary r_G by an R-matrix propagator method.[18] The essential approximation in the ADW method is to replace the R matrix at r_0 by the diagonal matrix constructed from logarithmic derivatives of regular functions $F_l(k,r_0)$. This is equivalent to neglecting all short-range potentials except the centrifugal and Coulomb terms used to define the functions F_l. This approximation becomes accurate for sufficiently large l at any given value of k. Results obtained are strictly unitary and are numerically accurate for a well-defined model described by long-range potentials cut off internally at r_0.

ADW calculations were carried out to examine the dependence of $K_{l'l}$ and K_{ll} on l. Results for $k = 10a_0^{-1}$ and $l = 10$, 20, and 30 are shown in Table I. Born approximation matrix elements $K_{ll}^{(B2)}$ and $K_{l'l}^{(B1)}$, $l' \neq l$, are included in the table, together with $K_{ll}^{(B1)}$(pol) from Eq. (14). These results demonstrate the internal consistency of using $K_{ll}^{(B2)}$ for diagonal elements and $K_{l'l}^{(B1)}$ for nondiagonal elements of the K matrix. With $r_0 = 1.0a_0$, short-range potentials are neglected in the Born-approximation matrix elements, since $kr_0 = 10$, while the potentials inside r_0 are set to zero in the ADW approximation. The good agreement of these two sets of results, even for $l = 10$, justifies use of the Born approximation for $l > kr_0$, especially when much higher l values must be considered.

Table I includes values of $K_{ll}^{(B1)}$(pol) for the static polarization potential. Clearly this is not a useful approximation to K_{ll} for $l \leq 30$. Since $l_B = 478$ for $k = 10a_0^{-1}$, this agrees with expectations, since the static polarization potential is not a good approximation to the optical potential in the range of r relevant to the l values considered in Table I.

The differences between ADW and Born-approximation results are insignificant at $l = 20$ and 30, but not negligible at $l = 10$, for the data shown in Table I. Even at $l = 10$, the error in the largest elements, $K_{l'l}$ for the dipole transition potential, is on the order of 10% while the K_{ll} element is small. In the calculations discussed below, $K_{ll}^{(B1)}$ for the static potential $v_{00}(r)$, which is much larger than $K_{ll}^{(B2)}$ for $l < kr_0$, is added into K_{ll}, so the relative error in $K_{ll}^{(B2)}$ is unimportant.

V. PARTIAL-WAVE BORN CALCULATIONS

K matrices were computed including elements $K_{ll}^{(B2)}$ and $K_{l'l}^{(B1)}$ for $l \geq kr_0$. For $l < kr_0$, $K_{ll}^{(B1)}(v_{00})$ was added in using Eq. (30), and elements $K_{l'l}^{(B1)}$ were scaled to account for short-range screening of the dipole transition

TABLE I. K-matrix elements computed by ADW and Born approximations $K_{pq}^{(B1)}$ if $p \neq q$, $K_{pq}^{(B2)}$ if $p = q$; $k = 10a_0^{-1}$.

	$l=10$		$l=20$		$l=30$	
p,q	ADW	Born	ADW	Born	ADW	Born
l,l	0.27736−3	0.19702−3	0.14714−3	0.14782−3	0.11879−3	0.11938−3
$l-1,l$	0.72696−1	0.81444−1	0.439848−1	0.43936−1	0.30575−1	0.30574−1
$l-1,l-1$	0.57917−2	0.83005−2	0.16379−2	0.17188−2	0.62002−3	0.64003−3
$l+1,l$	0.54078−1	0.56581−1	0.26107−1	0.26098−1	0.15903−1	0.15902−1
$l+1,l-1$	−0.50054−3	0.00	−0.26598−3	0.00	−0.15921−3	0.00
$l+1,l+1$	−0.60749−2	−0.57107−2	−0.15894−2	−0.15150−2	−0.67959−3	−0.65807−3
$K_{ll}^{(B1)}$(pol)		0.15405		0.20561−1		0.62351−1

potential. In preliminary calculations at 15 keV, K-matrix elements were computed on a grid of l values up to $l=2600$. T matrices were computed from these 3×3 K matrices, ensuring unitarity. The T-matrix elements were interpolated to l values between the grid points. The summation formula, Eq. (11), was used only for v_{00} (with $l_B=kr_0$) and for the static polarization potential (with $l_B=2600$). Equation (14) was found to be a reasonable approximation to $\mathrm{Re}T_{ll}$ for $l>2600$. These calculations were used to check the formalism and to verify convergence. In the final calculations reported here, Eq. (11) was used for $f_p^{(B2)}(\theta)$. Adequate convergence was found for $l\gtrsim kr_0$. The reported results used $l_B=100$, greater than kr_0 but much smaller than l_B required if Eq. (13) is to be used for $\Delta f^{(B1)}$(pol).

The static screened Coulomb potential of ground-state atomic hydrogen is given by $v_{00}(r)$, Eq. (8). To model other atoms, allowance must be made for different values of r_0, the atomic radius, and of f_{osc}, the oscillator strength contributing to inelastic electron scattering at given impact energy. If it is assumed that $r_0=a_0$ for hydrogen, and that all electrons not contributing to f_{osc} can be condensed with the nucleus into an effective point charge $+f_{\mathrm{osc}}$, the resulting model static potential is

$$v_{00}(r)=-\frac{f_{\mathrm{osc}}}{r_0}e^{-2r/r_0}(1+r_0/r)\ . \tag{31}$$

The first-Born-approximation scattering amplitude for $v_{00}(r)$, for elastic momentum transfer K_0, is

$$f_0^{(B1)}=\tfrac{1}{2}f_{\mathrm{osc}}r_0^2\left[\frac{1}{1+K_0^2r_0^2/4}+\frac{1}{(1+K_0^2r_0^2/4)^2}\right]\ . \tag{32}$$

In analogy to the use of Eq. (13) for the polarization potential, Eq. (12) is used in the present calculations to sum partial-wave scattering amplitude contributions from $v_{00}(r)$ for $l>kr_0$.

The residual sum of partial-wave amplitudes, Eq. (13), which determines the forward scattering peak, is directly proportional to the static dipole polarizability α. Electric dipole excitation at all energies is constrained by the sum rule, that total oscillator strength f_{osc} equals the number of electrons accessible in an excitation process. When all dipole excitation is concentrated in a single pseudostate, these two parameters are related to the reduced transition moment μ and excitation energy ΔE_p of the pseudostate by the formulas

$$\alpha=\tfrac{2}{3}\mu^2/\Delta E_p\ , \tag{33}$$

$$f_{\mathrm{osc}}=\tfrac{2}{3}\mu^2\Delta E_p\ . \tag{34}$$

In the present work, r_0 is taken to be $1.0a_0$ for hydrogen and $1.8a_0$ for argon, while α is given its experimental value ($4.5a_0^3$ for hydrogen, $11.07a_0^3$ for argon[19]). Two models have been used here for atomic hydrogen. Model 1 assumes

$$\Delta E_p^{(1)}=\tfrac{18}{43}=0.418\,60\ \text{a.u.}\ , \tag{35}$$

the excitation energy of the exact dipole pseudostate.[20] This implies, given $\alpha=4.5a_0^3$,

$$f_{\mathrm{osc}}^{(1)}=18\times(\tfrac{9}{43})^2=0.788\,53\ . \tag{36}$$

Model 2 adjusts ΔE_p to make $f_{\mathrm{osc}}=1$. The value is

$$\Delta E_p^{(2)}=0.471\,40\ \text{a.u.} \tag{37}$$

Results of calculations for e^- + H scattering at 15 keV are summarized in Table II and in Fig. 1. For comparison, Fig. 1 includes (graph $B2$) the second-Born-approximation elastic differential cross section computed from the pseudostate model.[4] The present results show a forward elastic peak (below 4 mrad) of essentially the same magnitude and shape as the $B2$ result. The difference in magnitude between the three calculations shown in Fig. 1 is due to different assumptions and approximations in the treatment of short-range potentials, which are not the principal concern of the present work. The main point established by the present calculations is that exact unitarization and reasonable changes of total oscillator strength and of the relative strength of short-range potentials have no significant effect on the magnitude and angular dependence of the forward elastic scattering peak, as computed in the second Born approximation.

Similar calculations were carried out with parameters intended to model atomic Ar. These parameters are

$$\begin{aligned}&\text{Model 1: } \alpha=11.07,\ f=2.029\,65,\ \Delta E_p=0.428\,19\ ,\\ &\text{Model 2: } \alpha=11.07,\ f=18.0,\ \Delta E_p=1.275\,15\ ,\end{aligned} \tag{38}$$

TABLE II. e^- + H scattering amplitudes at 15 keV. Differential cross sections in units a_0^2/sr.

θ	Model 1, $f_{\mathrm{osc}}=0.788\,53$			Model 2, $f_{\mathrm{osc}}=1.0$		
mrad	$\mathrm{Re}f(\theta)$	$\mathrm{Im}f(\theta)$	$d\sigma/d\Omega$	$\mathrm{Re}f(\theta)$	$\mathrm{Im}f(\theta)$	$d\sigma/d\Omega$
0	0.876 52	0.286 20	0.850 19	1.098 52	0.319 74	1.308 98
2	0.791 88	0.196 26	0.665 59	1.004 56	0.222 60	1.060 49
4	0.783 75	0.154 49	0.638 13	0.993 77	0.179 38	1.019 75
6	0.776 50	0.130 73	0.620 04	0.984 44	0.152 46	0.992 37
8	0.767 39	0.114 14	0.601 92	0.972 85	0.133 70	0.964 31
10	0.756 19	0.101 43	0.582 11	0.958 63	0.119 33	0.933 20
12	0.742 98	0.091 14	0.560 33	0.941 86	0.107 70	0.898 70
14	0.727 93	0.082 52	0.536 69	0.922 77	0.097 96	0.861 10
16	0.711 25	0.075 13	0.511 52	0.901 61	0.089 61	0.820 93
18	0.693 16	0.068 67	0.485 19	0.878 67	0.082 31	0.778 84
20	0.673 90	0.062 96	0.458 11	0.854 25	0.075 85	0.735 49

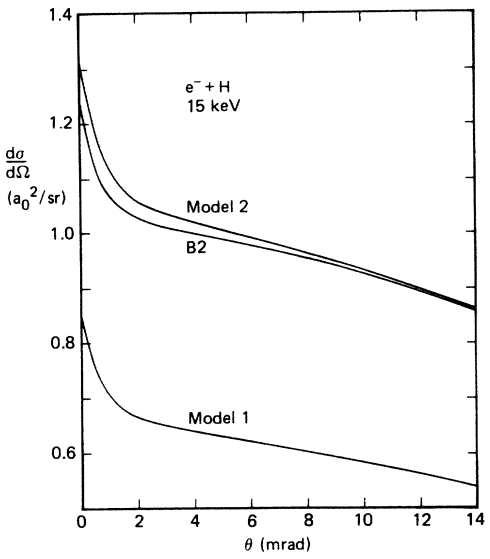

FIG. 1. H-atom models: differential elastic cross section in the forward direction.

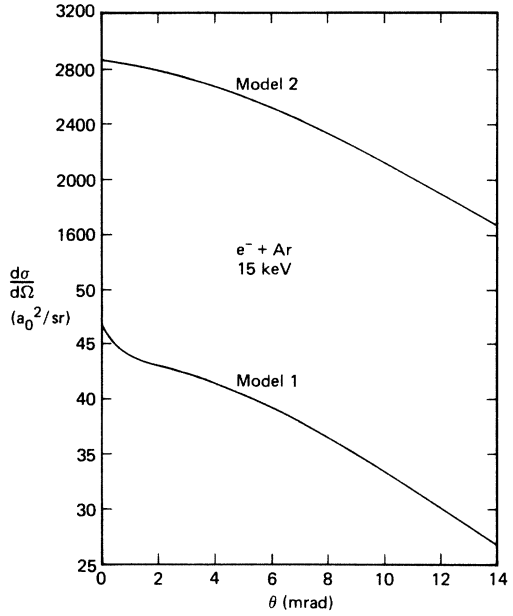

FIG. 2. Ar-atom models: differential elastic cross section in the forward direction.

all in atomic units. In model 1, the pseudostate excitation energy is that of the dipole-allowed transition $3p \rightarrow 4s$, which limits the oscillator strength to the small value shown. Model 2 is an extreme alternative, associating the observed static polarizability with the excitation of all 18 electrons.

Results of these calculations are given in Table III and in Fig. 2. At 15 keV, in model 1, the forward peak is similar in shape and in angular extent to that found for hydrogen. In model 2, the forward peak is hardly visible because of a much larger shorter-range background, which contains a large contribution from the model static potential, Eq. (31). In both cases the extreme forward peak is small relative to the background.

A generalized optical theorem follows directly from Eq. (A12). This is built into the present results through use of the closure formula, Eq. (11), for $f_p^{(B2)}(\theta)$. For $e^- + H$, models 1 and 2, and for $e^- + Ar$, model 1, the differential cross sections shown in Figs. 1 and 2 are closely approximated by the first-Born-approximation cross section for the static potential for angles greater than 4 mrad. From Eq. (32), $f^{(B1)}(0)$ is $f_{osc} r_0^2$, which determines the relative magnitudes of the cross sections in the different models. In the case of $e^- + Ar$, model 2, $v_{00}(r)$ is so large that unitarity corrections reduce the magnitude of the computed cross section to roughly 10% below first Born approximation.

VI. DISCUSSION AND CONCLUSIONS

The principal result of the present work is to verify for $e^- + H$ scattering in the keV energy range that the second-Born-approximation elastic scattering amplitude is substantially correct at very small scattering angles. Hence, the qualitative implications of exact calculations[4] of $f^{(B2)}(\theta)$ for a pseudostate model of atomic hydrogen are supported. It appears not to be possible to interpret recent experimental data[1,2] showing a forward elastic peak

TABLE III. $e^- + Ar$ scattering amplitudes at 15 keV. Differential cross sections in units a_0^2/sr.

θ	Model 1, $f_{osc} = 2.029\,65$			Model 2, $f_{osc} = 18.0$		
mrad	Re$f(\theta)$	Im$f(\theta)$	$d\sigma/d\Omega$	Re$f(\theta)$	Im$f(\theta)$	$d\sigma/d\Omega$
0	6.777 57	0.822 20	46.6115	52.0933	12.6007	2872.49
2	6.533 41	0.599 32	43.0447	51.3486	12.3745	2789.81
4	6.419 10	0.494 01	41.4489	50.3013	12.0814	2676.18
6	6.251 15	0.433 94	39.2652	48.8026	11.8546	2522.23
8	6.030 80	0.391 88	36.5241	46.8592	11.6624	2331.80
10	5.767 63	0.359 49	33.3948	44.5479	11.4837	2116.39
12	5.472 87	0.333 13	30.0632	41.9649	11.3077	1888.91
14	5.157 76	0.310 91	26.6991	39.2085	11.1288	1661.16
16	4.832 63	0.291 69	23.4394	36.3699	10.9438	1442.54
18	4.506 37	0.274 76	20.3828	33.5273	10.7511	1239.67
20	4.186 14	0.259 64	17.5912	30.7440	10.5497	1056.49

much stronger than the $f^{(B1)}$ background, to be the result of single elastic collisions between electrons and ground-state atoms. The discrepancy of roughly two orders of magnitude between $f^{(B2)}(\theta)$ and partial-wave calculations by Mohr,[9] who used a similar model for hydrogen at 35 keV impact energy, remains unexplained.

The present parametric treatment of short-range potentials is not intended to be quantitatively accurate. The simplified formulas used here make calculations feasible for a wide range of parameters. In the case of $e^- + \mathrm{Ar}$ scattering, this flexibility has been used to consider two extreme excitation models. In both cases, the incremental forward elastic scattering peak is small compared with the background, due primarily to the short-range static potential. This indicates that qualitative conclusions based on exact second-Born-approximation calculations for a pseudostate model of hydrogen are valid for rare-gas atoms in general.

The present partial-wave calculations are unitarized by constructing the T matrix for each l value from a real symmetric K matrix. Except at low l values, effects of unitarization are found to be negligible. The effects of different treatments of the short-range potentials are much more important.

In the present calculations, numerical solutions of the coupled differential equations of the pseudostate model merge smoothly into partial-wave Born-approximation results for high l values. For $l > kr_0$, where r_0 is an effective atomic radius, exact Born-approximation amplitude calculations and partial-wave Born-approximation calculations using asymptotic potentials are found to be compatible. Amplitude $f_0^{(B1)}$ for the static potential and $f_p^{(B2)}$ for the asymptotic dipole transition potential provide accurate summation formulas to complete truncated partial-wave expansions.

The present calculations show that elastic scattering at high impact energies is described by a cusplike forward peak in the differential cross section, superimposed on a more smoothly varying background due to the short-range static potential. This peak is described by $f_p^{(B2)}(\theta)$, given explicitly here by Eq. (A15). In the present examples, since $f_p^{(B2)}$ is small compared with the static scattering amplitude $f_0^{(B1)}$, the forward peak in the differential cross section arises primarily from the cross term between $\mathrm{Re}f_p^{(B2)}$ and $f_0^{(B1)}$, so that $\mathrm{Im}f_p^{(B2)}$ does not contribute significantly. Moreover, since $\mathrm{Im}f(\theta)$ varies quadratically with momentum transfer K_0, cusp behavior (linear variation with K_0) occurs only in $\mathrm{Re}f(\theta)$.

The present analysis identifies this forward cusp with the residual partial-wave sum due to the asymptotic polarization potential, given here by Eq. (13). For impact energies above the excitation threshold ΔE_p the excitation process reduces the magnitude of matrix elements $\mathrm{Re}T_{ll}$ below values appropriate to the static polarization potential, given by Eq. (14). This effectively removes terms $l < l_B$ from the partial-wave sum for l_B estimated by Eq. (18), leaving the residual amplitude $\Delta f(\theta)$ of Eq. (13) as an approximation to $\mathrm{Re}f_p(\theta)$.

Both Eqs. (13) and (A15) can be expanded about $K_0 = 0$ in the form

$$\mathrm{Re}\Delta f(\theta) = \pi a(ck - \tfrac{1}{4}K_0) + O(K_0^2) . \tag{39}$$

From Eq. (A15), the constant c is

$$c(B2) = \Delta E_p / 2k^2 \tag{40}$$

and from Eqs. (14) and (15),

$$c(\mathrm{pol}) = \frac{1}{3} - \sum_{l=1}^{l_B} \frac{1}{(2l+3)(2l-1)} \tag{41}$$

$$= \sum_{l>l_B} \frac{1}{(2l+3)(2l-1)} . \tag{42}$$

If Eq. (13) is to be used by itself to approximate $\mathrm{Re}f_p^{(B2)}(\theta)$, l_B should be determined by equating $c(B2)$ and $c(\mathrm{pol})$. This results in the estimate

$$l_B \cong \frac{k^2}{2\Delta E_p} , \tag{43}$$

smaller than Eq. (18) but with the same dependence on energy parameters.

Equation (39) establishes the essential behavior of the forward elastic scattering peak. Incremental magnitude (above the short-range background) and initial slope with respect to momentum transfer are proportional to the static polarizability. From Eq. (40), the magnitude decreases with increasing impact energy.

Experimental data on electron scattering by rare-gas atoms, indicating a forward elastic peak much larger than found here for models of H and Ar, cannot be reconciled with the present results for ground-state atoms. However, since the magnitude of the forward peak is proportional to μ^2, where μ is the reduced transition moment, a much larger effect might be observed if a significant population of excited atoms were present. For Rydberg states μ^2 scales as n^4 for principal quantum number n. For atomic hydrogen, a relative population of 2×10^{-2} in the $n=3$ states would produce a larger contribution to the forward elastic cross section than does unit population in the ground state.

From Eq. (A15) and the optical theorem, similarly large factors affect the total inelastic cross section for scattering by excited atoms. The measured differential elastic cross section would depend on the relative steady-state population of excited atoms in the beam path. Two recent crossed-beam experiments[21,22] have failed to reproduce the forward elastic scattering enhancement reported by Geiger and Morón-León.[1] These new results agree with theory for scattering by ground-state atoms. However, they do not rule out possible observation of excited atoms or ions under different experimental conditions.

ACKNOWLEDGMENTS

Both authors are grateful for the hospitality of the University of Kaiserslautern, West Germany, where this project was initiated with the support of Sonderforschungsbereich 91. S.G. acknowledges support by the Alexander von Humboldt Foundation. Work at IBM San Jose Research Laboratories was supported in part by the U.S. Office of Naval Research.

APPENDIX A: SECOND BORN APPROXIMATION FOR THE DIPOLE EXCITATION POTENTIAL

Following standard definitions and analysis,[23] the indirect second-Born-approximation elastic scattering amplitude, due to the μ/r^2 off-diagonal potential in Eq. (15), is

$$f_p^{(B2)}(\theta) = \frac{1}{2\pi^2}\lim_{\epsilon\to 0+}\int \frac{d^3\mathbf{q}}{q^2-k_p^2-i\epsilon}\sum_m [f_{pm}^{(B1)}(\mathbf{t}')]^* f_{pm}^{(B)}(\mathbf{t}) , \tag{A1}$$

where

$$f_{pm}^{(B1)}(\mathbf{t}) = -\frac{2\mu}{\sqrt{3}}\frac{i}{t}\left[\frac{4\pi}{3}\right]^{1/2} Y_{1m}^*(\hat{\mathbf{t}}) , \tag{A2}$$

with

$$\mathbf{t}=\mathbf{k}-\mathbf{q}, \quad \mathbf{t}'=\mathbf{k}'-\mathbf{q} , \tag{A3}$$

for incident electron momentum $\mathbf{k}$ and final momentum $\mathbf{k}'$. Using

$$\sum_m Y_{1m}(\hat{\mathbf{t}}')Y_{1m}^*(\hat{\mathbf{t}}) = \frac{3}{4\pi}\frac{\mathbf{t}\cdot\mathbf{t}'}{tt'} \tag{A4}$$

and the definition of momentum transfer,

$$K_0^2 = 4k^2\sin^2(\theta/2) , \tag{A5}$$

Eq. (A1) reduces to

$$f_p^{(B2)}(\theta) = \frac{\mu^2}{3\pi^2}\int \frac{d^3\mathbf{q}}{q^2-k_p^2-i\epsilon}\frac{t^2+(t')^2-K_0^2}{t^2(t')^2} . \tag{A6}$$

Equation (A6) can be evaluated in terms of Dalitz integrals.[23-25] The integrals required here, defined by

$$Q_I(p,\lambda,\kappa) = \frac{1}{\pi^2}\int \frac{d^3\mathbf{q}}{q^2-p^2-i\epsilon}\frac{1}{[(\mathbf{q}-\boldsymbol{\kappa})^2+\lambda^2]^I} , \tag{A7}$$

depend only on the magnitude of $\boldsymbol{\kappa}$ and are

$$Q_1(p,\lambda,\kappa) = \frac{i}{\kappa}\ln\left[\frac{p+\kappa+i\lambda}{p-\kappa+i\lambda}\right] , \tag{A8}$$

$$Q_2(p,\lambda,\kappa) = \frac{1}{\lambda(\kappa^2+\lambda^2-p^2-2p\lambda i)} . \tag{A9}$$

In terms of these integrals,

$$f_p^{(B2)}(\theta) = \frac{\mu^2}{3}\left[2Q_1(k_p,0,k) - K_0^2\int_0^1 du\, Q_2(k_p,\lambda(u),\kappa(u))\right] , \tag{A10}$$

where

$$\lambda^2(u) = K_0^2 u(1-u) , \qquad \kappa^2(u) = k^2 - K_0^2 u(1-u) . \tag{A11}$$

The final integral in Eq. (A10) can be evaluated analytically[26] to give

$$f_p^{(B2)}(\theta) = \frac{\mu^2}{3}\left\{\left[\frac{2\pi}{k}-\frac{K_0\pi}{S}\right] + i\left[\frac{2}{k}\ln\left[\frac{k+k_p}{k-k_p}\right] - \frac{K_0}{S}\ln\left[\frac{S+k_pK_0}{S-k_pK_0}\right]\right]\right\} , \tag{A12}$$

where

$$S^2 = (k^2-k_p^2)^2 + k_p^2K_0^2 . \tag{A13}$$

Partial-wave analysis of Eqs. (A1) and (A2) gives a form of the generalized optical theorem

$$\mathrm{Im}f_p^{(B2)}(\theta) = \sum_{l=0}^{\infty}\frac{2l+1}{k}\sum_{l'=l\pm1}|T_{l'l}^{(B1)}|^2 , \tag{A14}$$

where the left-hand term is given by Eq. (A12) and matrix elements $T_{l'l}^{(B1)}$ are defined by Eq. (23).

In the high-energy limit, the closure approximation for $f_p^{(B2)}$ gives[6,7]

$$f_p^{(B2)}(\theta) = \frac{\mu^2}{3}\left\{\left[\frac{\pi}{k}-\frac{K_0\pi}{S}\right] + i\left[\frac{1}{k}\ln\left[\frac{k+k_p}{k-k_p}\right] - \frac{K_0}{S}\ln\left[\frac{S+k_pK_0}{S-k_pK_0}\right]\right]\right\} , \tag{A15}$$

which differs from Eq. (A12) by reducing the coefficient of Q_1 in Eq. (A10) to unity. This difference can be traced to the present use of the singular unscreened form μ/r^2 for the dipole transition potential in Eqs. (5). When the smooth cutoff given by Eq. (9) is included, numerical values of $f_p^{(B2)}$ agree with Eq. (A15) rather than with Eq. (A12). These two formulas are equivalent when used as closure formulas for partial-wave sums, since they differ only by a term independent of scattering angle. Since nonsingular transition potentials occur in any physical application of this formalism, Eq. (A15) should be used in preference to Eq. (A12). The agreement between forward scattering structures computed here (model 2) and calculations using the nonsingular transition potential (B2), as shown in Fig. 1, verifies that use of Eq. (A15) does not introduce an error here.

APPENDIX B: TRANSITION MATRIX ELEMENTS IN THE PARTIAL-WAVE BORN APPROXIMATION

From Eqs. (6) and (24), Eq. (23) can be expressed as

$$T_{l'l}(k_p,k) = -\frac{2\mu}{\sqrt{3}}\left[\frac{l_>}{2l+1}\right]^{1/2} \times \int_0^\infty dr\frac{1}{r}J_{l'+1/2}(k_pr)J_{l+1/2}(kr) , \qquad l'=l\pm1 . \tag{B1}$$

The integral here is known[27] in the form of the product of a constant and a hypergeometric function. Using an integral representation of the hypergeometric function[27] for $l'=l-1$, and with $z=k_p^2/k^2$ so that $z<1$,

$$T_{l-1,l}(k_p,k)=-\frac{\mu}{[3l(2l+1)]^{1/2}}\left[\frac{k_p}{k}\right]^{l-1/2} \times\int_0^1 lt^{l-1}\left[\frac{1-zt}{1-t}\right]^{1/2}dt\ . \tag{B2}$$

The final integral here is evidently greater than or equal to unity, approaching this limit when $z=1$. The integrand is positive definite. In the present work this integral is evaluated numerically after removing the singularity at $t=1$ by transforming the integration variable to $x=(1-t)^{1/2}$.

For $l'=l+1$,

$$T_{l+1,l}(k_p,k)=-\frac{\mu}{[3(l+1)(2l+1)]^{1/2}}\left[\frac{k_p}{k}\right]^{l+3/2} \times\int_0^1 dt\frac{1}{2t^{1/2}}\left[\frac{1-t}{1-zt}\right]^{l+1}\ . \tag{B3}$$

In this case, the final integral is less than or equal to unity, approaching this limit when $z=1$. This integral is evaluated numerically after transforming to $x=t^{1/2}$. It obviously becomes very small for large l, so that $T_{l+1,l}$ vanishes relative to $T_{l-1,l}$ for large l. This behavior is expected in the classical limit, since an incident classical electron that loses linear momentum at large impact parameter in forward scattering must also lose angular momentum.

In preliminary calculations used to verify Eqs. (A12) and (A14), $\mathrm{Re}T_{ll}^{(B2)}$ (or $K_{ll}^{(B2)}$) was evaluated directly from Eq. (21) by numerical integration of the principal-value integral.[28] The integrand requires values of $T_{l',l}(k',k)$ for general values of k'. If $k'\le k$, Eqs. (B2) and (B3) are valid. If $k'>k$, interchanging l and l' in Eq. (B1) leads to the same formulas, with k and k' interchanged.

From Eqs. (B2) and (B3), $T_{l'l}(k',k)$ varies as a high power of $k_</k_>$ on both sides of $k'=k$ for large l. In the limit of very large l this causes the integrand of Eq. (21) to be dominated by values near $\epsilon'-\epsilon$ (or $k'=k$) so that Eq. (21) approaches Eq. (14) for large l.

In the final calculations reported here, both $\mathrm{Re}T_{ll}^{(B2)}$ and $\mathrm{Im}T_{ll}^{(B2)}$ were computed by Eq. (29). The quadrature interval $(-1,+1)$ was first mapped onto itself, superimposing intervals $(-1,0)$ and $(0,+1)$ at mirror points. Then the range (0,1) was divided geometrically into n subintervals

$$(0,\tfrac{1}{2}),\ldots,(1-2^{-n+3},1-2^{-n+2}),(1-2^{-n+2},1-2^{-n+1}),(1-2^{-n+1},1)\ . \tag{B4}$$

Calculations with 48 Gauss quadrature points in each of ten subintervals appeared to converge to eight significant decimals for values of l up to 100.

For values of $l<kr_0$, $T_{l'l}$ should be modified to take into account the effect of the short-range screening potential, Eq. (9). Since analytic formulas are not available, a simple approximation was used in the present work. If screening is assumed to reduce the integrand of Eq. (B1) to zero for $r<r_0$, then for small l and sufficiently large k, asymptotic expressions can be used for the spherical Bessel function factors. This leads to the formula

$$T_{l'l}\cong[l_>/(2l+1)]^{1/2}\times\text{const}\ , \tag{B5}$$

which was used in the present work for $l<kr_0$, with the constant determined from $T_{l'l}$ for $l=kr_0$.

APPENDIX C: MATRIX ELEMENTS OF THE STATIC POTENTIAL

The scattering amplitude $f_0^{(B1)}(\theta)$ for the model static potential $v_{00}(r)$ of Eq. (31) is given by Eq. (32). The corresponding partial-wave transition matrix elements are

$$T_{ll}^{(B1)}=\frac{2f_{\mathrm{osc}}}{r_0}\int_0^\infty dr\,r^2kj_l^2(kr)e^{-2r/r_0}(1+r_0/r) \tag{C1}$$

$$=\frac{2f_{\mathrm{osc}}}{k}\left[h(l,1,\beta)+\frac{1}{kr_0}h(l,2,\beta)\right]\ , \tag{C2}$$

where

$$h(l,n,\beta)=\int_0^\infty dz\,j_l^2(z)z^ne^{-\beta z}\ . \tag{C3}$$

It is convenient to break Eq. (C3) into two integrals

$$h(l,n,\beta)=h_{\mathrm{I}}+h_{\mathrm{II}}\ , \tag{C4}$$

where

$$h_{\mathrm{I}}(l,n,\beta)=\int_0^l dz\,j_l^2(z)z^ne^{-\beta z}\ , \tag{C5}$$

$$h_{\mathrm{II}}(l,n,\beta)=\int_l^\infty dz\,j_l^2(z)z^ne^{-\beta z}\ . \tag{C6}$$

For $z>l$, $j_l(z)$ can be computed accurately as a finite sum of inverse powers of z multiplying $\sin z$ and $\cos z$. Hence h_{II} is a sum of real and complex exponential integral functions, and was evaluated in this form in the present work. The inner integrals h_{I} have monotonically increasing integrands. They were computed by numerical quadrature after converting to the integration variable

$$t=(z/l)^{n+l+1}\ . \tag{C7}$$

This has the effect of smoothing the rapid power law variation of the integrand.

[1]J. Geiger and D. Morón-León, Phys. Rev. Lett. **42**, 1336 (1979).

[2]O. Müller and J. Geiger, in *Proceedings of the Thirteenth International Conference on the Physics of Electronic and Atomic Collisions* (ICPEAC, Berlin, 1983), p. 81.

[3]S. Geltman and R. K. Nesbet, in *Proceedings of the Thirteenth International Conference on the Physics of Electronic and Atomic Collisions* (ICPEAC, Berlin, 1983), p. 82.

[4]S. Geltman and R. K. Nesbet, Phys. Rev. A **30**, 1636 (1984).

[5]H. R. J. Walters, Comments At. Mol. Phys. **5**, 173 (1976); A. M. Ermolaev and H. R. J. Walters, J. Phys. B **12**, L779 (1979).

[6]R. A. Bonham, Phys. Rev. A **3**, 298,1958 (1971); R. A. Bonham and S. Konaka, J. Chem. Phys. **69**, 525 (1978).

[7]F. R. Byron, Jr. and C. J. Joachain, Phys. Rev. A **8**, 1267 (1973); J. Phys. B **10**, 207 (1977).

[8]F. W. Byron, Jr. and C. J. Joachain, J. Phys. B **14**, 2429 (1981).

[9]C. B. O. Mohr, J. Phys. B **2**, 166 (1969).

[10]R. K. Nesbet, J. Phys. B **17**, L897 (1984).

[11]P. G. Burke, I. Mackey, and I. Shimamura, J. Phys. B **10**, 2497 (1977).

[12]D. G. Thompson, Proc. R. Soc. London, Ser. A **294**, 160 (1966).

[13]P. G. Burke and H. M. Schey, Phys. Rev. **126**, 147 (1962).

[14]M. Gailitis, J. Phys. B **9**, 843 (1976).

[15]R. K. Nesbet, Abstracts, Fifth West Coast Theoretical Chemistry Conference, Abstract No. 87 (SRI Intl., Menlo Park, California, April 1983) (unpublished).

[16]R. K. Nesbet, *Variational Methods in Electron-Atom Scattering Theory* (Plenum, New York, 1980), p. 100.

[17]C. J. Noble and R. K. Nesbet, Comput. Phys. Commun. **33**, 399 (1984).

[18]K. L. Baluja, P. G. Burke, and L. A. Morgan, Comput. Phys. Commun. **27**, 299 (1982).

[19]T. M. Miller and B. Bederson, Adv. At. Mol. Phys. **13**, 1 (1977).

[20]R. Damburg and E. Karule, Proc. Phys. Soc. London **90**, 637 (1967).

[21]J. D. Coffman, M. Fink, and H. Wellenstein, Phys. Rev. Lett. **55**, 1392 (1985).

[22]S. N. Ketkar and R. A. Bonham, Phys. Rev. Lett. **55**, 1395 (1985).

[23]C. J. Joachain, *Quantum Collision Theory* (North-Holland, Amsterdam, 1975).

[24]R. H. Dalitz, Proc. R. Soc. London, Ser. A **206**, 509 (1951).

[25]R. P. Feynman, Phys. Rev. **76**, 769 (1949).

[26]R. R. Lewis, Jr., Phys. Rev. **102**, 537 (1956).

[27]*Handbook of Mathematical Functions,* edited by M. Abramowitz and I. A. Stegun (Natl. Bur. Stand. Appl. Math. Ser. No. 55) (U.S. GPO, Washington, D.C., 1964).

[28]H. Morawitz, J. Comput. Phys. **6**, 120 (1970).